RESEARCH PAPER

Enhancement of joint properties and reduction of intermetallics in FSW of highly dissimilar Al/Ti alloys

Saed Enam Mustafa[1] [ORCID] · **Rajiv Nandan Rai[1]** · **Raashid Firoz[2]**

Abstract

In this research work, welding of highly dissimilar aluminum alloy (6061-T6) and titanium alloy (Ti6Al4V) has been carried out using copper (Cu) interlayer with the friction stir welding (FSW) process by varying the tool rotation speed and tool traverse speed. FSW is a welding technique in which the plates to be joined are plastically deformed due to friction by a non-expendable rotating tool and welded as the tool traverses along the length of the plates. In the absence of any interlayer, the welded joint of the alloys, as mentioned above, failed along the joining surface due to the formation of the intermetallics, leading to low strength and brittleness. High strength and good quality joints are obtained using a Cu interlayer between the two alloys and a tapered tool at a lower tool rotation speed, and traverse speed due to appropriate deformation, uniform mixing, and effective temperature rise during welding. Also, using the interlayer between the Al and Ti alloys enhanced the joint strength by reducing the formation of Al_3Ti intermetallic. Other non-optimal conditions resulted in wormhole defects and intermetallics formation, thus resulting in degraded joint quality and strength. The joint welded at optimum welding conditions failed in a pure ductile manner, while the others were either in hybrid or brittle mode. Tool rotation and traverse speeds are found to be crucial for proper mechanical mixing as they impact the weld's structure, phase development, and mechanical characteristics. Furthermore, the optimal process parameters were validated with the help of ANOVA.

Keywords Friction stir welding · Dissimilar metals · Intermetallics · Interlayer · ANOVA

1 Introduction

Joining dissimilar metals has wide applications in many industries, such as aviation, marine, defense, and locomotives [1, 2]. Weight and cost reduction of manufactured units with enhanced output is demandable to maximize the throughput in industries and compete in the global market [3]. Assembly of aluminum (Al) and titanium (Ti) alloys is highly applicable in the aerospace industries, where an increase in the strength-to-weight ratio is a significant prerequisite [4]. For example, in aircraft production, the fuselage of an airplane is joined by skin-stringer joints, seating tracks, heat exchangers, and welding of aluminum skins to titanium ribs aircraft. Aluminum has high strength, is light in weight, is cheap, and can easily deform. Titanium is tough, non-corrosive, and has a high melting point and strength. Due to balancing attributes, these two materials are extensively used in various structural parts [5].

On the other hand, successfully joining dissimilar metals such as titanium and aluminum alloys is quite challenging as the two alloys have huge contrast in mechanical, chemical, and metallurgical properties [6]. There have been several attempts to weld these two metals in the past. Various welding techniques, for instance, ultrasonic welding [7], MIG welding [8], laser welding [9], and cladding [10], have been attempted. However, the traditional processes have various complications, such as the compulsion for a gas shield, welding equipment, and geometrical restrictions of the welds [7, 9, 11]. The most important phenomenon for failure is the formation of brittle intermetallics in the Al/Ti joint [11]. Wei et al. [12] established the vacuum diffusion joining of

✉ Saed Enam Mustafa
semustafa@iitkgp.ac.in

1 Subir Chowdhury School of Quality and Reliability, Indian Institute of Technology Kharagpur, Kharagpur 721302, West Bengal, India

2 Department of Metallurgical and Materials Engineering, Indian Institute of Technology Kharagpur, Kharagpur 721302, West Bengal, India

titanium and aluminum alloys. This research work investigated that $TiAl_3$ intermetallic composite was developed in the diffusion bonding of pure Ti–Al joints [13]. Friction welding of Ti–6Al–4 V and AA5052 round bars was carried out, but the joints cracked with the development of $Ti_2Mg_3Al_{18}$ intermetallics in the weld region [14].

FSW, an innovative welding technique established by The Welding Institute (TWI) in 1991, is a possible option for joining difficult-to-weld alloys. Since its establishment, the friction stir weld method has gained wide recognition as a high-quality welding method for the automotive, ship manufacturing, and aerospace industries [15]. FSW is an environmentally friendly and green welding technique that often eliminates the use and evolution of harmful gases and substances [16]. Green production has recently gained significant importance by reducing hazardous discharges, eliminating waste, and reutilizing resources [17]. FSW is conducted using a revolving tool that plastically deforms the adjacent material to produce the joint with considerable heat [18], as shown in Fig. 1. It has wide applicability and potential to prevent the formation of hard and brittle intermetallics at the joint. FSW solves the problem of joining similar metals [19], different metals, and incompatible metals [20].

Dissimilar friction stir lap joining of pure Al and Ti was reported with Al_3Ti forming at the interface of the Al/Ti diffusion process [21–26]. Dressler et al. [27] concluded that friction stir butt welding could effectively weld Al/Ti alloys. AA6061 and Ti6Al4V alloys with high thickness were welded with a novel tool. The joint strength was only 35% of Al alloy [3]. The poor weld strength was caused by insufficient stirring. It was reported that the Al_3Ti layer continuously existed along the joint of AA6061 and Ti alloy
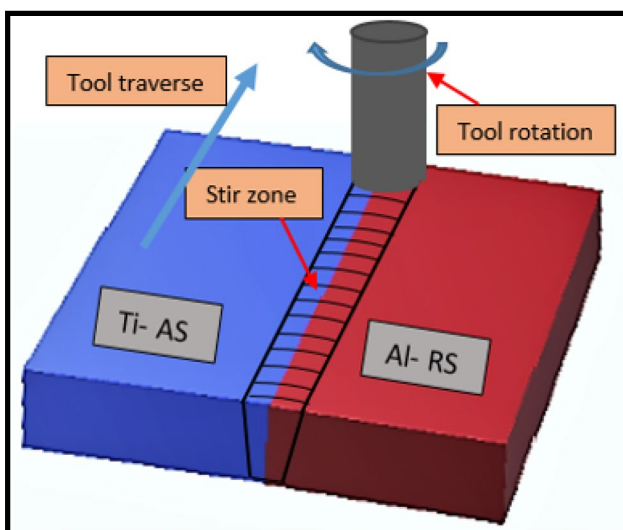
welds [13]. It was also found that during welding, a higher tool offset leads to the formation of more Al/Ti intermetallics and weld cracks along the joining area [28]. However, the growth of Al/Ti intermetallics at the joining surfaces remains problematic as it reduces the quality of the joint [29, 30]. The joint cracked near the interface of Al and Ti due to the development of Al_3Ti [31].

In order to mitigate the formation and influence of unwanted intermetallics, the use of different interlayers has been proposed by various researchers in FSW of different metals and alloys [32–36]. The welding of AA6061 to AISI 4340 was conducted using a silver interlayer, and the thickness of intermetallics was reduced, thereby enhancing the tensile strength [37]. Excellent bonding between Ti alloy and stainless steel (SS) without cracks and preventing significant martensitic changes were achieved using a Cu interlayer [38]. Different interlayers were used in FSW of wrought Al that shifted the fracture position from the advancing side (AS) to the retreating side (RS) by forming a composite mixture and increasing the strength [39]. Silver was used in laser welding–brazed dissimilar Al and Ti, and it was found that the incompatibility between the metals was reduced by the reduction of $TiAl_3$ [40]. In another study, Ti-mesh interlayer was used in laser welding–brazed Al and Ti, in which more $TiAl_3$ was found at the joints, increasing the weld's microhardness [41]. FSW of Al and Ti alloys with zinc foil in the middle was investigated, but the joint became more brittle due to Zn0.69Ti0.31 intermetallic in the weld area [42]. In another study, an Al_2O_3 nanoparticle was used as reinforcement in FSW of Al and Ti, and defect-free was obtained due to the pinning effect and thermal stability of the process, which limited the growth of intermetallics at the joint interface [43].

Abdollah-Zadeh et al. [44] carried out the friction stir butt welding (FSBW) of AA1060 with pure Cu. It was found that the intermetallics of Al and Cu were less brittle than that of Al and Ti. During the FSW of AA1060 with pure Cu, the intermetallics mainly formed were Al_2Cu, Al_4Cu_9, and AlCu, and the joints had excellent properties with good strength [45, 46]. It was also established that at temperatures predicted during FSW (approx. 410 °C), Cu is more soluble in aluminum than in titanium. Hence, Al_aCu_b and Cu_cTi_d compounds are less brittle and harder in the welded region than Al3Ti intermetallics. Moreover, since the melting point of copper is (~ 1050 °C), which is higher than that of Al (~ 670 °C) and lower than that of Ti (~ 1665 °C). Therefore, according to the rule of mixture, Cu is expected to improve the quality of the Al/Ti alloy welded joints with respect to physical properties and microstructure evolution [47]. In Al/Ti welding, the production of Al_3Ti is unavoidable and takes place at a specific temperature. In the FSW of aluminum, selecting an appropriate interlayer with base metals proved necessary to manage rotating force and temperature [48].

Fig. 1 Schematic diagram of the FSW process with the tool traverse and rotation directions

The interlayer used in the research work had a lower melting temperature than the FSW processing temperature and melted during the process. As a result, the processing load and torque increased, but the welding temperature decreased. In this context, researchers further investigated the microstructure and physical characteristics of pure Al and Ti in FSW with niobium (Nb) as a middle layer under particular welding conditions [5]. Nb acted as an excellent middle layer to delay the production of the Al_3Ti intermetallics by restricting the interaction between pure Al and Ti. Another study found that Cu as a middle layer reacts with pure Al and Ti to form a solid solution and an intermetallic Al_2Cu [47].

Elemental mixing in weld nuggets and the development of intermetallics are controlled by the tool's location and faying contact between aluminum and titanium [49], while other factors, such as tool rotational speed and welding speed, are also primarily accountable [50]. From the literature review, the research gaps that can be enumerated are as follows:

1. Most Al/Ti alloys have been welded by the FSW process without any interlayer, where intermetallics' growth significantly reduces the joint strength.
2. FSW of Al and copper has been performed, and it was found that the intermetallics formed were less brittle than that of Al/Ti joints, so the use of Cu as an interlayer in FSW of Al and Ti could help improve the joint quality.
3. FSBW of pure Al and Ti plates had also been studied with the addition of pure Cu as interlayer with only the tool offset as a variable parameter, whereas other factors, such as rotational tool speed and welding speed, have not been explored. Also, the work on validating optimal process parameters through statistical tools is limited in the FSW of dissimilar joints with interlayers.
4. Various attempts have been made to diminish the formation and growth of intermetallics in welding different metallic alloys under different processes. However, the intermetallics reduction by interlayers in FSBW of AA6061 T6 and Ti6Al4V alloys has not been studied.

Considering the literature gaps and wide industrial applications as discussed earlier, the investigation conducted in this paper aims to enhance the joint properties by reduction of intermetallics with the use of Cu interlayer and determination of optimal process parameters such as tool rotation speed and traverse speed in FSBW of AA6061-T6 and Ti6Al4V alloys with interlayers.

This present research work focuses on mitigating the formation of intermetallics with the application of copper interlayer. The enhanced weld properties of the Al-Ti joints were confirmed with the uniaxial tensile tests and microhardness measurements.

2 Experimental details

2.1 Materials and method

In this research work, AA6061 T6 aluminum alloy and Ti6Al4V titanium alloys with dimensions 150 mm × 75 mm × 3 mm were used in a single-pass butt joint. Pure copper foil (99% above) with 200 μm thickness was used as interlayers. The edges of the plates to be welded were rubbed through emery paper to remove any burr present due to shear cutting and then cleaned with acetone for degreasing. The K-type thermocouples were attached to the plate at a distance of 15 mm from the edge on the Al side and 10 mm on the Ti side as the tool was mainly on the Al side due to offset, as shown in Fig. 2. Ti was placed on the advancing side (AS), and aluminum on the retreating side (RS) since a higher temperature is produced on the AS. Then, the plates were appropriately fixed with the help of fixtures. The chemical and physical characteristics of the materials are given in Tables 1 and 2, respectively.

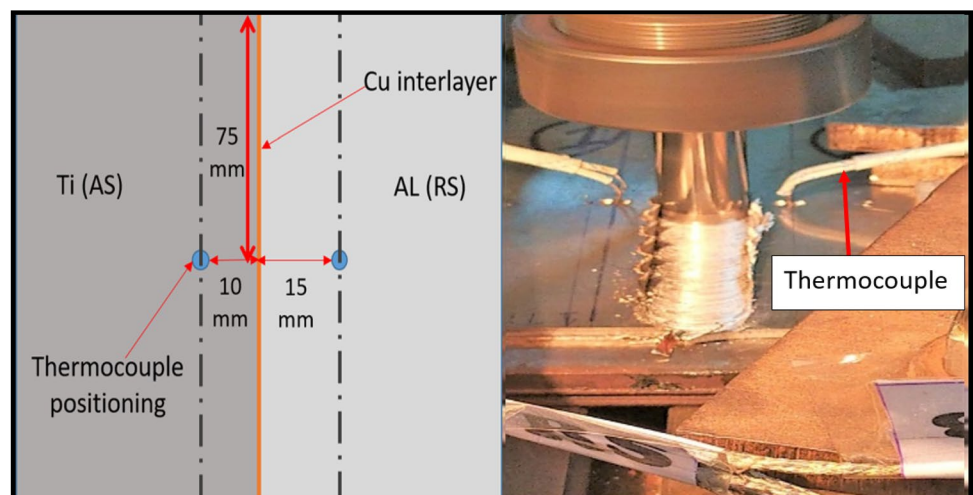**Fig. 2** Schematic diagram of the positioning of thermocouples on both Al and Ti sides during FSW

Table 1 Chemical constituents (%) of Al and Ti alloy

	Si	Mg	Cu	Fe	C	Al	Ti	V
AA6061-T6	0.623	1.000	0.220	0.110	-	Bal	0.039	-
Ti-6Al-4 V	-	-	-	0.048	0.053	5.76	90.14	3.69

Welding parameters such as tool rotation speed (rpm), tool traverse speed (TS), and tool offset (TOF) were selected as variables for trial experiments. Both the cylindrical and tapered tools were tested for welding at various conditions based on available sets in the machine, such as (rpm-500, 710, 1000, 1400, and 2000), (TS-14, 20, 28, 40, and 56 mm/min), and (TOF-0.5, 1.0, and 1.5 mm) respectively. The trial experiments found the combination of three rotation speeds (500, 710, and 1000 rpm) and three traverse speeds (14, 20, and 28 mm/min) suitable as input variables. The tapered tool only with a 1.0 mm offset on the titanium side was appropriate for experimenting. A constant tool plunge depth of 0.2 mm was maintained throughout the experiment. The FSW input parameters and values considered in this research work are summarized in Table 3. One coupon was tested for each welding condition. A total of nine coupons were welded under different conditions, as provided in Table 4.

2.2 FSW machine and tool setup

The experimental setup comprises a modified milling machine with a 7.5 hp motor to carry out the FSW experiments, as shown in Fig. 3. The tool was mounted in the tool holder using a suitable collate, and a particular fixture has been used to carry out the experiments [51]. The machine consists of a low carbon steel plate of about 250 mm × 350 mm to place the welding samples. To one side of the plate, nuts were fixed to help fasten the bolts for fixing the welding plates tightly. The other side of the plate had a welded metal bar fixed, which acted as a barrier to the sample plates—the machine bed slots to hold the welding samples from the top position. The collate in which the tool is fixed for welding is gripped firmly inside the tool holder.

The experiments were conducted with the help of tools made of a tungsten carbide rod with 10% cobalt. It has a 70 mm long shoulder and 18 mm dia., with the face tapered by one degree, and two types of tool pins (Fig. 4 a and b) of 2.8 mm length were considered. Tools with a cylindrical pin had a diameter of 6 mm, and a tapered pin had 6 mm and 4 mm diameters at the root and tip, respectively. Both the cylindrical and tapered tools were tested through trial experiments. A tapered tool with the tip positioned at 1 mm offset towards the Ti side was found suitable for experimentation. The schematic diagram with dimensions and positioning of the plate and tool is shown in Fig. 5.

2.3 Microstructural and mechanical characterizations and statistical study

In order to determine the quality of the welded joints, based on the literature [6, 15, 29, 30, 52], the tests carried out in this research work are the welding temperature, phase evolution, microstructural development, hardness variation, tensile strength, and morphology of fractured surfaces. One sample for microstructural investigation and microhardness testing, two for tensile tests, and one for X-ray diffraction (XRD) analysis were sectioned from each coupon, as shown in Fig. 6, with the help of a wire-cut electrical discharge machining. The samples for microhardness and microstructure were cut normal to the weld direction and then polished using various grades of emery paper. Specimens were polished on both sides with different grades of emery papers (400 to 2000 grades). For microstructural characterization, the mirror-like finish was given on one side of the sample using cloth polishing with

Table 2 Physical characteristics (%) of Al and Ti alloy [28]

	Yield strength (MPa)	UTS (MPa)	Elongation (%)
AA6061-T6	289	318	11.2
Ti-6Al-4 V	877	952	12.6

Table 3 FSW input parameters and their levels with values

Parameters	Level 1	Level 2	Level 3
Rotation speed (rpm)	500	710	1000
Traverse speed (mm/min)	14	28	40
Tool pin offset (mm)	1	1	1
Tool pin type	Tapered	Tapered	Tapered

Table 4 Experiment design matrix for the full-factorial experiment

Samples no	Rotation speed (rpm)	Welding speed (mm/min)
S1	500	14
S2	500	20
S3	500	28
S4	710	14
S5	710	20
S6	710	28
S7	1000	14
S8	1000	20
S9	1000	28

Fig. 3 FSW setup used for welding: a modified milling machine, b nomenclature of different parts
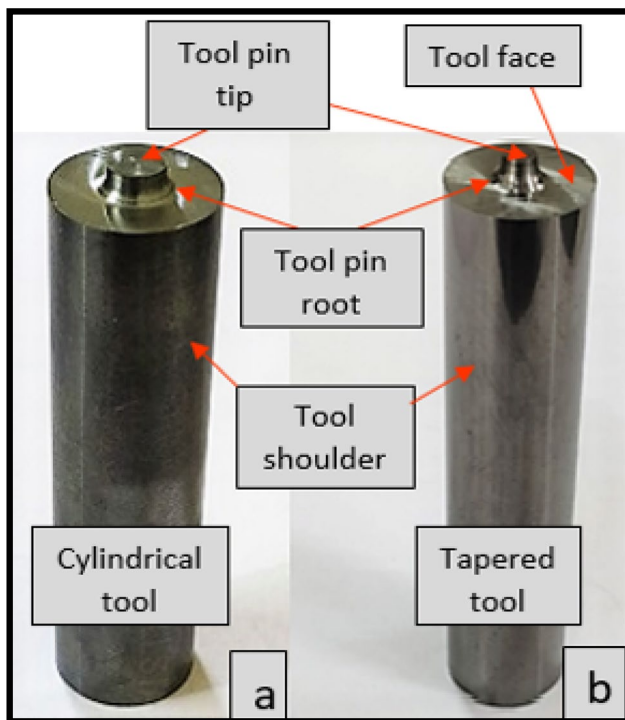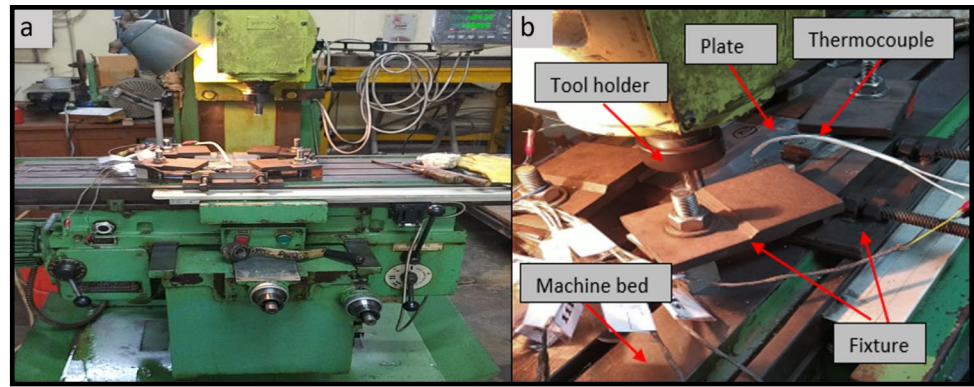

Fig. 4 Types of tools used for experiments: a cylindrical tool and b tapered tool

different grades of diamond, such as 6 microns, 2 microns, 1 micron, and 0.25 microns. Afterward, the welded samples were etched with Keller's and Kroll's reagents for 5 s for aluminum and titanium, respectively. The process of polishing and etching was repeated several times to obtain optimum etching and desired quality of the images. An optical microscope (Leica microsystems DFC295, Germany) was used to perceive the macrostructure and microstructure of the welded joints at different magnifications. Scanning electron microscope (SEM) analysis was done through (Zeiss Sigma 300 VP, UK). For hardness, cloth polishing was done on the other side of the sample. Hardness testing was performed using a Vickers microhardness tester at 500 g load for 10 s.

The tensile specimen had a 10 mm width, 6 mm gauge thickness, 36 mm gauge length, 100 mm overall length, and 3 mm thickness, as depicted in Fig. 7. These dimensions were taken per the standard ASTM E8M-04 specifications. The samples were knurled at the front and back of both the Ti and Al sides with the help of metallic files and then tested on a universal testing machine (Tinius Olsen H50KS, UK). Finally, the validation of optimal process parameters was carried out with the help of ANOVA.

3 Results and discussion

3.1 Microstructural analysis of welded joints

In this subsection, Fig. 8 depicts microstructures of the joint at varied welding conditions such as S1 (rpm-500, TS-14 mm/min), S4 (rpm-710, TS-14 mm/min), and S9 (rpm-1000, TS-28 mm/min). The constituent aluminum, titanium, and copper are shown in the image with symbols. The difference in the mixture of the triplets at different welding conditions can be seen in the welded zone. The copper element can be seen in the joining region of samples S4 and S9, as in Fig. 8(c, d, e, and f). Two regions are displayed for each sample; namely, tool pin-assisted region (TPAR), shown in Fig. 8(a, c, and e), and tool-shoulder-assisted region (TSAR), established in Fig. 8(b, d, and f).

Figure 8(a and b) shows the macrostructure of the joint of sample S1 at the welding conditions (rpm-500, TS-14 mm/ min). A large proportion of mechanical mixture concerning sample S4 (rpm-710, TS-14 mm/min) is shown in Fig. 8(c and d). Uncrushed copper is not visible at the joining region in Fig. 8(a and b). Figure 8(f) displays the microstructure of the joint of sample S9 at welding parameters (rpm-1000, TS-28 mm/min). Compared to the other two welds of samples S1 and S4, sample S9 exhibits a violent mechanical mixture in the tool-shoulder-aided distortion zone. Furthermore, the mechanically mixed area has a meager percentage of elemental Cu, as depicted by the contrast of the

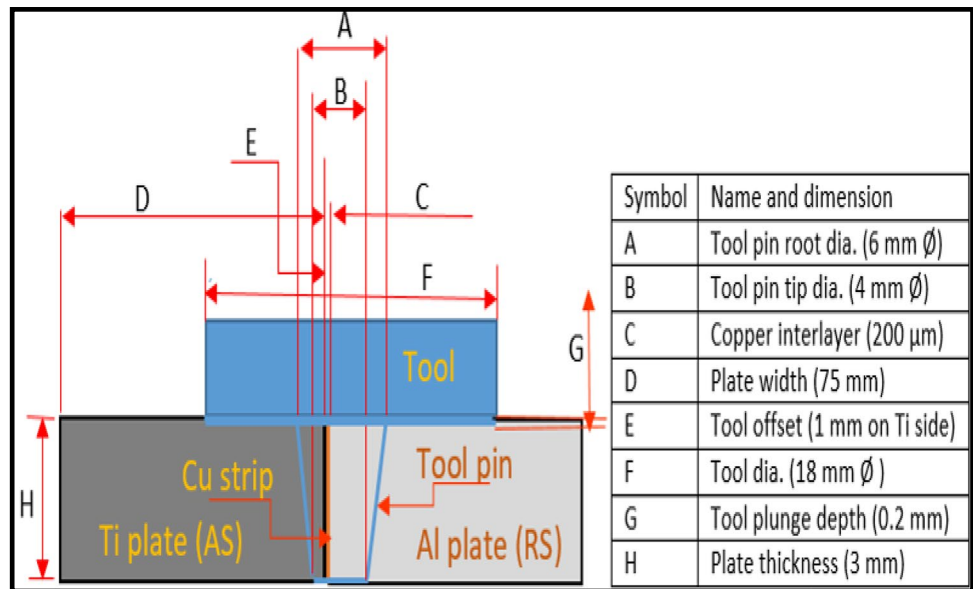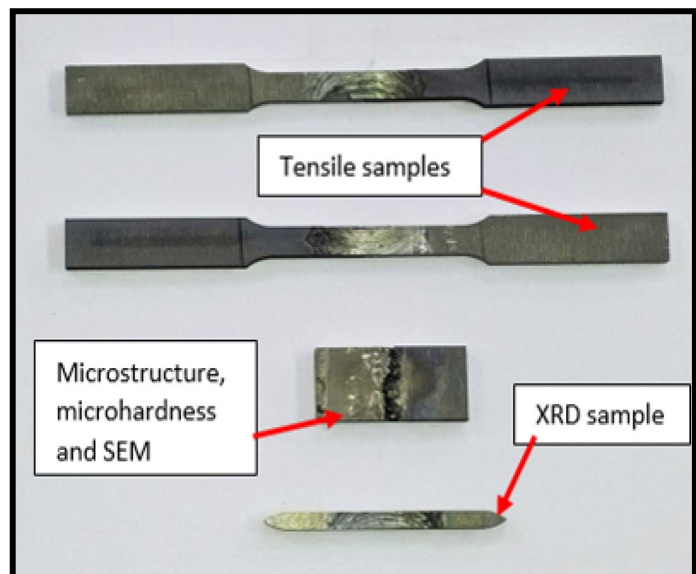**Fig. 5** Schematic diagram showing the dimensions and positioning of the plates and the tool

Symbol	Name and dimension
A	Tool pin root dia. (6 mm Ø)
B	Tool pin tip dia. (4 mm Ø)
C	Copper interlayer (200 μm)
D	Plate width (75 mm)
E	Tool offset (1 mm on Ti side)
F	Tool dia. (18 mm Ø)
G	Tool plunge depth (0.2 mm)
H	Plate thickness (3 mm)

Fig. 6 Sectioned samples for microstructural and mechanical characterization

microstructures. Additionally, a significant amount of void is seen around the connecting contact at the base of the joint. Tool rotation, traverse speed, and tool pin size determine how materials are deformed and mechanically mixed. The tool interacts well with Ti and the Cu interlayer at lower tool rotation and traverse speeds. Therefore, proper mechanical mixing is noticed at (rpm-500, TS-14 mm/min). An inadequate and inappropriate mixture is observed in the welded region of samples S4 (rpm-710, TS-14 mm/min) and S9 (rpm-1000, TS-28 mm/min), correspondingly. The copper layer present at the joint of S4 (rpm-710, TS-14 mm/min) is due to the decreased contact of the tool with copper.

Conversely, a large proportion of Al and void in the welded region of sample S9 (rpm-1000, TS-28 mm/min)

indicate insufficient interaction and severe distortion. Near the TSAR and the faying area, there is significant distortion and an abundance of voids. The deformation and improper mixing resulting at this higher setting of rpm and TS are seen in Fig. 8(f). The resulting weld nugget has an uneven distribution of material and erratic flow. The movement of the soft Al would be challenging if the weld nugget contained hard, undistorted titanium particles. Parting or void is anticipated at the region of such hard particles when they move in a softer matrix flow. The weld nugget would develop a void due to this flow separation. These voids are seen in Fig. 8(e and f). As the drift in the welded region is restricted by the un-deformed titanium particles, the material cannot press force against

Fig. 7 Details of the samples sectioned for tensile testing
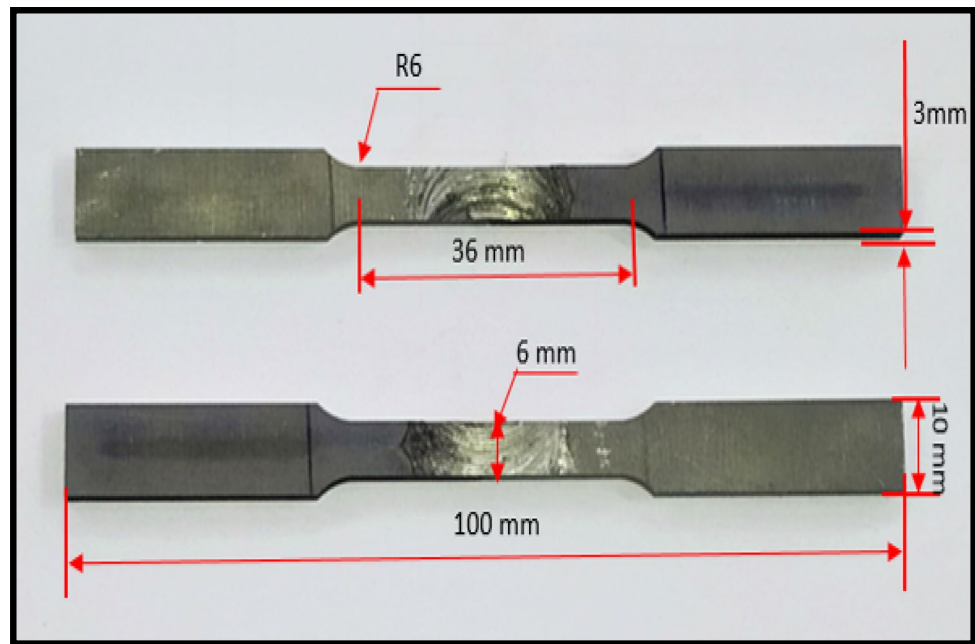
AS, resulting in the development of a wormhole and void. The joint of sample S1 (rpm-500, TS-14 mm/min) is moderately mixed and deformed and, therefore, is defect-free concerning other joints.

The SEM image of the joint transverse section of sample S1 (rpm-500, TS-14 mm/min), as shown in Fig. 9(a), comprises the elements of copper, titanium, and aluminum alloys. A large proportion of elemental copper is seen. These constitute the mechanical mixing region (MMR) of the welded zone. The joining interface in Fig. 9(b) shows an intermediate layer, denoted by the letter *b* in Fig. 9(a). The contrast in the image shows how interstitial particles develop and how Al and Ti are mechanically mixed. As seen in Fig. 9(c), the weld nugget exhibits a distinct mechanical mixing. The image displays a variety of particles with different interlayer thicknesses at their surrounding interfaces. Additionally, it is also visible that the aluminum matrix contains elements of various sizes. Back-scattered SEM has been preferred to examine the detailed interfacial characteristics associated with the weld of sample S1 (rpm-500, TS-14 mm/min).

Figure 10(a) depicts a less magnified microstructure of the joint of samples S4 welded at (rpm-710, TS-14 mm/min) through back-scattered scanning electron microscopy (BSE-SEM). Al, Ti, and Cu can be distinguished by the image contrast, as seen in the figure. It is interesting to note that Ti does not deform at the joining area. However, a small proportion of the copper at the upper portion of the joint is deformed, resulting in tiny fragments of Cu scattered in the welded zone. Figure 10(b) shows the joining region designated as *b* in Fig. 10(a). The interface does not develop an intermediary layer. A wormhole is visible in the region next to the copper layer (Fig. 10(c)). Figure 11(a) shows scanned microstructures from the joint of sample S9 welded at (rpm-1000, TS-28 mm/min). It demonstrates how the materials were severely mixed and deformed. The weld nugget exhibits various flaws, as seen in Fig. 11(b). The interfaces between two MMRs are where these flaws are most noticeable (Fig. 11(b, c)). Additionally, the weld includes particles of various sizes. A close examination indicates that defects mainly occur next to big, elongated particles in contrast to smaller particles.

The copper fragments in the welded zone are smaller in size than titanium. The development of flaws in the welded zone is dependent on welding conditions. The root defects in the weld sample S9, which was welded at (rpm-1000, TS-28 mm/min), resulted from inadequate Ti deformation and contact with the tool pin. Due to increased tool rotation and traverse speed, the tool starts vibrating and interacts violently with the titanium and copper layer while welding. These interactions lead to undesirable MMRs in the welded zone and in-between layer. The best welding conditions, which have an impact on mechanical mixing, are essential for the formation of regulated intermediate layers. When the parameters are higher than optimal, excess mixing may result in formation defects. A weld with few defects is anticipated when the welding settings are optimized (rpm-500, TS-14 mm/min) since flow separation is reduced and leads to the filling up of defective zones.

Fig. 8 Macrostructure images of the tool pin-assisted and tool-shoulder-assisted regions of different FSW welded samples: a, b sample S1, c, d sample S4, and e, f sample S9
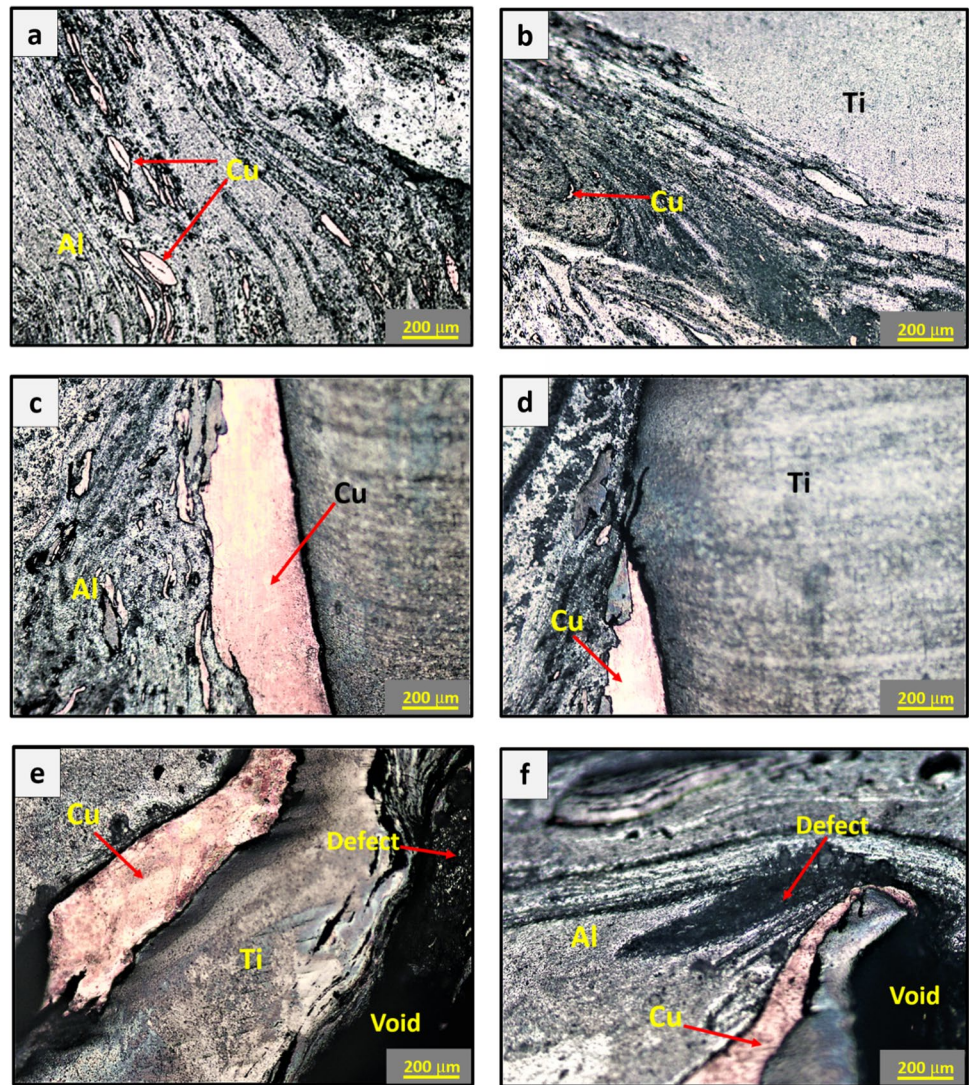
3.2 XRD analysis

X-ray diffraction has been done to identify the evolution of phases in different samples. Figure 12 shows XRD patterns from the weld of samples S1, S9, and S0. The weld region was positioned in the middle of the XRD radiation to determine the development of phases in the welded zone. The intermetallic combination of Al_3Ti in the weld in the absence of a Cu interlayer was detected, as denoted by the peaks of sample S0. No such significant peak indicating intermetallic compounds was observed in the welds of sample S1 (rpm-500, TS-14 mm/min). The adequate mixing in the weld and the used interlayer was responsible for the defect-free joint.

In contrast, peaks indicating a considerable amount of intermetallics were observed in the sample S9 welded at 1000 rpm and TS-28 mm/min. The growth of defects and intermetallic evolution are accordingly constrained by optimal deformation and temperature evolution. Excess mixing and following thermal diffusions are responsible for the development of intermetallics.

Compared to Al and Ti welding without an interlayer, copper as an interlayer material produces less brittle intermetallic (Al_3Ti) due to the screening of Al with Ti. Two critical factors affecting intermetallic development at the junction of Al and Ti are welding duration and temperature [53]. It was found that the thickness of Al_3Ti and morphology are influenced by the amount of heat used during gas arc welding of Al to Ti and by laser welding [54]. Contrarily, in methods such as diffusion welding [55], ultrasonic welding [7], and FSW, the temperature rises due to the process, and the period of the welding process influences the type of intermetallics and the joint structure. Conversely, it was stated that the Al/Ti junction is susceptible to the growth of Al_3Ti regardless of the welding and joining methods employed [56]. In addition

Fig. 9 **a** SEM image of the welded sample S1, **b** intermediate layer, and c mechanically mixed region (MMR)
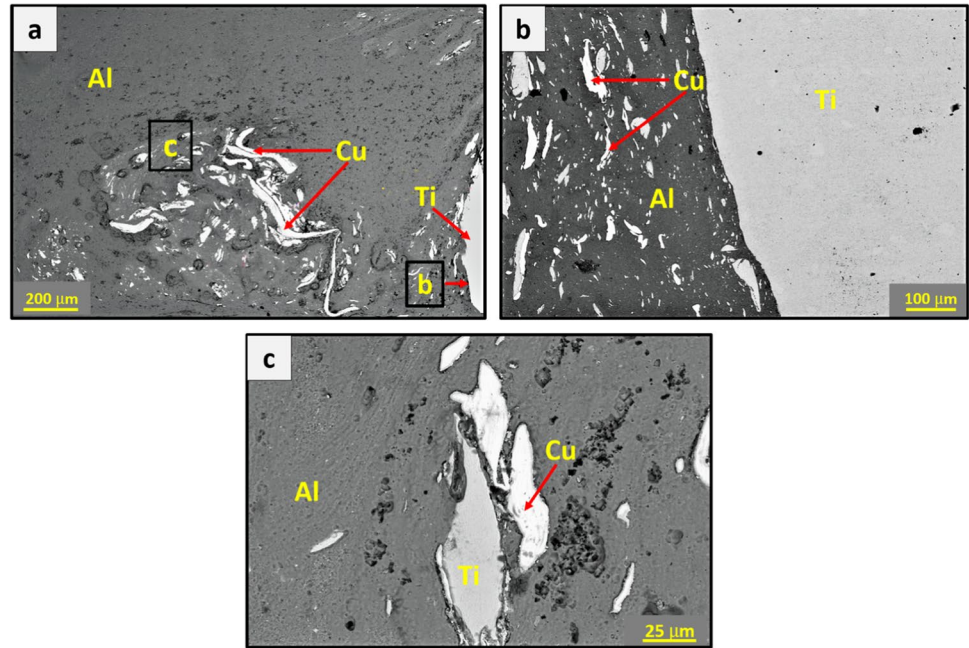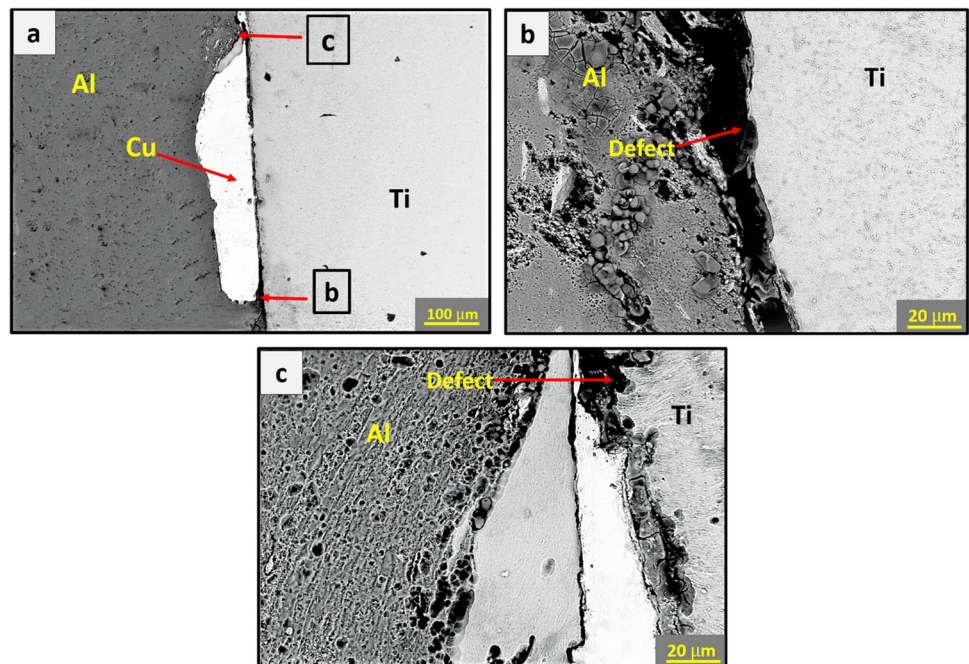

Fig. 10 **a** SEM image of welded sample S4, **b** intermediate layer, and **c** mechanically mixed region

to the thickness, the structure of intermetallics and distribution can significantly impact weld characteristics.

3.3 Microhardness measurements

The hardness profiles of the cross-section of the joints of all the welded samples representing the titanium side, the central region, and the aluminum side are shown in Fig. 13. The hardness is nearly 371 HV on the Ti side of the weld of sample S1

(rpm-500, TS-14 mm/min). Higher welding parameters resulted in turbulent mixing in the weld region. It led to large flakes of copper mixed into the welded area, reducing the hardness on the titanium side. Consequently, there is a considerable decline in hardness to around 102 HV at the joining area of Ti and Al alloy (near AL alloy hardness). Hardness is not homogeneous near welded zone. It is higher near the joining area due to the fragmented Ti alloy mixed in Al alloy. This hardness increases at the highest speed (1000 rpm) because more Ti is fragmented

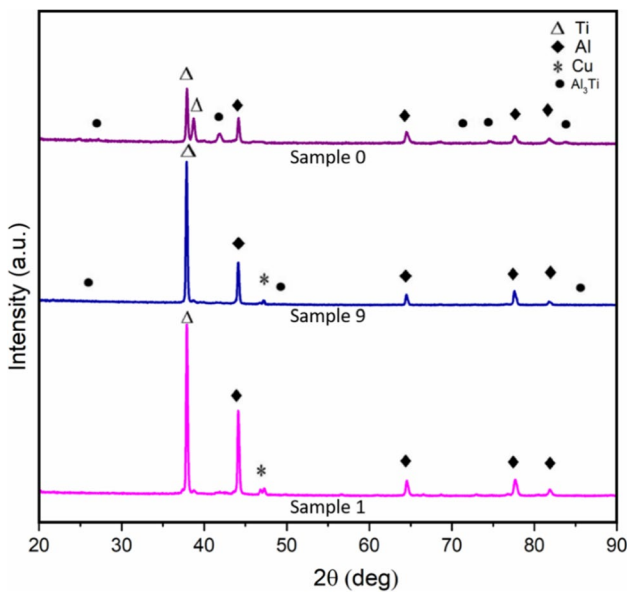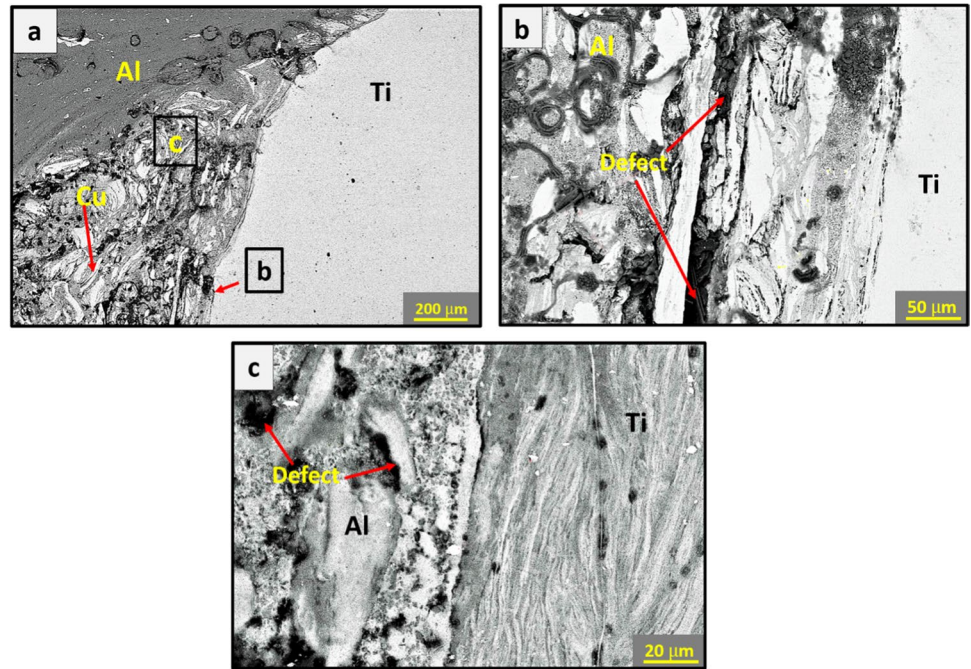**Fig. 11 a** SEM image of the weld of sample S9, **b** intermediate layer, and **c** mechanically mixed region

Fig. 12 X-ray diffraction analysis of the joint of three samples, S1, S9, and S0

Fig. 13 Hardness profiles of the transverse section of all the welds

into the welded zone than at 710 rpm. Due to the softening effect of FSW in precipitation-hardened aluminum alloys, the hardness near the Al alloy side in the welded zone is less than the base Al alloy [57]. The increased hardness on the aluminum side of the sample welded without a copper layer is observed because Al_3Ti is developed, which is hard and brittle [52].

3.4 Temperature profile

The development of phases is determined by Gibb's free energy of development of different phases at different temperatures. The expected intermetallic formed by joining aluminum and titanium is Al_3Ti, $AlTi$, and $AlTi_3$. It was found that since the brittle intermetallic phase Al_3Ti has the minimum Gibbs free energy of development between 100 and 1450 °C, it is predicted to emerge during welding [58]. Less diffusion time and higher temperature lead to the formation of Al_3Ti. In dissimilar metals, temperature difference and temperature rise are crucial factors in forming

defect-free joints in FSW. In the present experiment, the welding temperature on the Ti side and the temperature difference (between Al and Ti side) of the weld of sample S1 are recorded as 324 °C and 64 °C, respectively.

In comparison, both the factors in sample S9 are observed as 407 °C and 114 °C, as depicted in Fig. 14. Sample S1 exhibits a balanced mixture without any noticeable defect and contains negligible brittle intermetallics. Due to the existence of Cu, it forms an Al–Cu solid solution, leading to superior mechanical properties, as shown in the following sections. Defects such as voids and intermetallics are developed at temperatures below 450 °C as in sample S9 (1000 rpm, TS-28 mm/min)
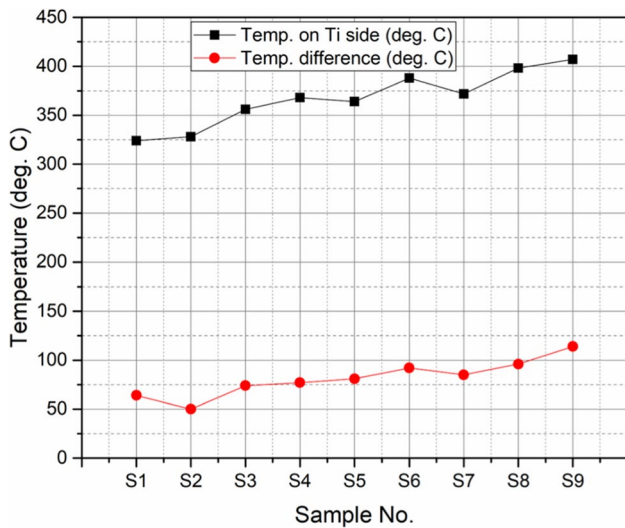

Fig. 14 Welding temperature on the Ti side and temperature difference (between Al and Ti sides)

shown in Fig. 11. These defects are not observed in the weld of sample S1 (500 rpm, TS of 14 mm/min). On the other hand, the intermetallic (Al_3Ti) and voids are formed in all the other welds due to insufficient diffusion time, higher welding temperatures, and differences, and it is maximum in sample S9.

3.5 Tensile test properties

The tensile strength of welded samples at welding conditions is shown in Fig. 15(a). The tensile strength of sample S1 welded at (500 rpm, 14 mm/min TS) was the best, followed by S2 and others. Therefore, one sample of the welded joint without a Cu interlayer under the same experimental condition was also prepared and denoted as S0 for a comparative study. The joint properties are determined by the interactions of the elements that form the intermetallics at the welded zone. The weld of sample S1 (rpm-500, TS-14 mm/min) subjected to moderate mixing and deformation gives better UTS than all other welded samples. At 500 rpm, the strength of the welds with TS of 14 mm/min and 20 mm/min is correspondingly 234 MPa and 219 MPa. As discussed in previous sections, because of the development of a few intermetallics and the proper mixing of Cu with Al and Ti alloys in the MMR, the use of copper as an interface layer in welded region inhibits the formation of hard and brittle Al_3Ti intermetallic by the formation of less brittle and harder Al_aCu_b and Cu_cTi_d compounds, thereby leading to the achievement of higher tensile strength. Also, the joints fractured in heat-affected zone, where the hardness is less (Figs. 16 and 17).

Weld strength reduces because of insufficient mixing and development of intermetallics at the tool rotation speed beyond 500 rpm. At 710 rpm, the weld strength with TS
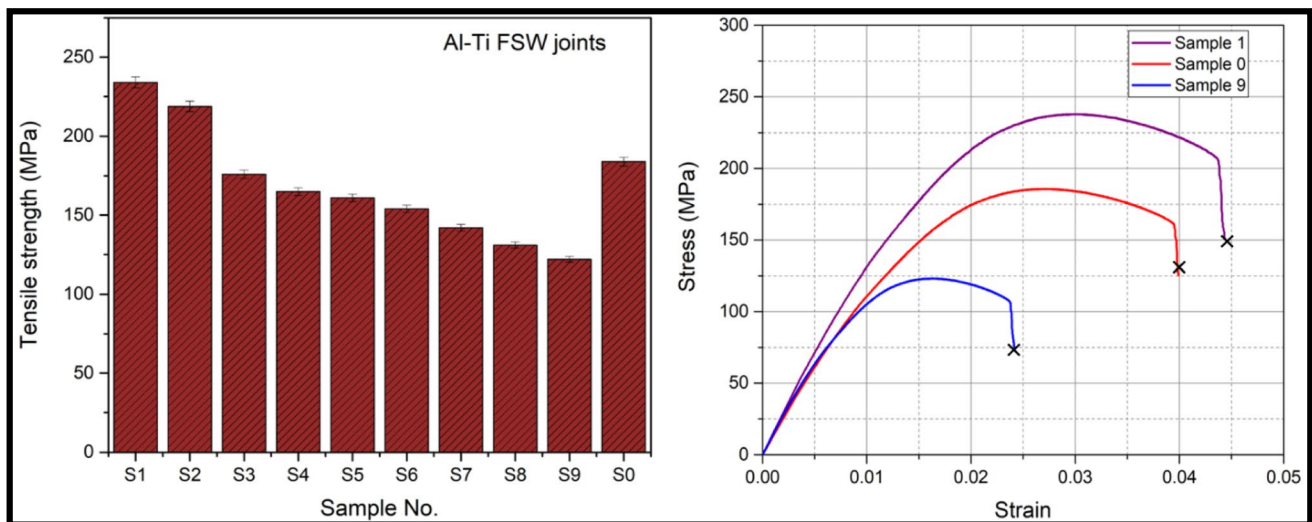

Fig. 15 a Variation of tensile strength at welding conditions, **b** S–S curve of samples S1, S9, and S0
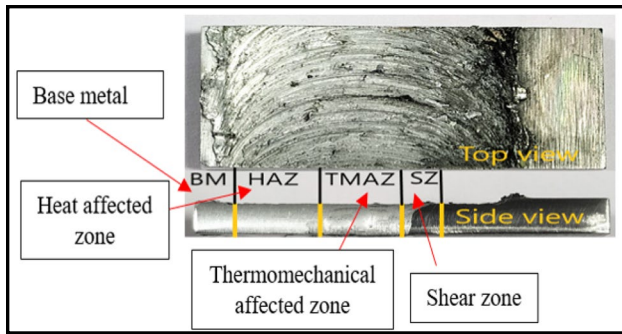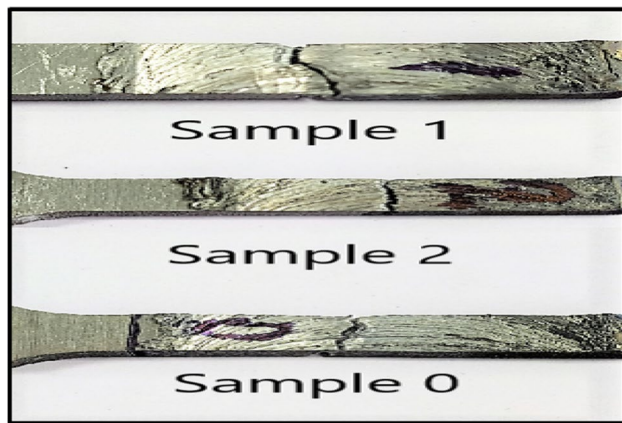
Fig. 16 Various regions found in a welded sample

Fig. 17 Crack position of failure of tensile specimens S1, S2, and S0 (between TMAZ and HAZ)

Fig. 18 Crack position of failure of tensile specimen S3 to S9 (between HAZ and SZ)

of 14 mm/min and 20 mm/min is at about the same level; however, as TS reaches 28 mm/min, the strength of the joint falls sharply. At 1000 rpm, the tensile strength decreases to 122 MPa, and the weld ruptures alongside the joining area. It can be attributed to more voids and intermetallics, as discussed in detail in previous sections. The samples S1 and S2 welded at (rpm-500, TS-14, and 20 mm/min) with Cu interlayer recorded the maximum tensile strength followed by S0 (184 MPa) because of fewer cavities and defects. The remaining samples showed lower joint strength due to flaws and intermetallics persisting in the welds. The stress vs. strain curve for samples S1, S9, and S0 is mentioned in Fig. 15(b).

It was investigated that the joints formed in welding Al and Ti alloys are due to intermetallics [59]. Figure 16 shows various regions found in a welded sample, namely base metal (BM), heat-affected zone (HAZ), thermomechanical affected zone (TMAZ), and stir zone (SZ). Figure 17 shows that the welded joints of samples S1, S2, and S0 fractured at the interface of TMAZ and HAZ because of differences in microstructures [60]. Most of the welded samples fractured at the border of SZ and TMAZ, as shown in Fig. 18. It is attributed to the plunging action, which

concentrates the stresses by decreasing the thickness and inadequate mixing and development of intermetallics.

3.6 Fractography analysis

The SEM images of the fracture surface of sample S1 are displayed in Fig. 19(a). The samples fractured along the Al side of the TMAZ and HAZ border and exhibited maximum tensile strength. It is a pure ductile fracture, according to the fractographic image (Fig. 19(b)). The presence of disseminated copper fragments in the depressions shows shear in the welded zone. Figure 20(a and b) depicts the BSE-SEM of the fractures of specimen S4 at low and high magnification. The fractured grain morphology is not tensile with few intermetallics, resulting in poor weld strength. In some regions of Fig. 20(a), the failure surface is smooth and free of significant distortion. Figure 21(a, b) shows the BSE-SEM images of sample S9. There were also voids with no metallurgical bonding. A few grains are shattered, indicating mixed grains (Fig. 21(b)).

Figure 22 depicts the BSE-SEM images of sample S0. Even though some Ti fragment is detected on the aluminum alloy side, it is evident that the cracks are brittle because of the development of intermetallics with the weld failing at the interface of HAZ and TMAZ on aluminum alloy.

The SEM–EDX results of the fractured samples S1, S4, S9, and S0 are shown in Fig. 23. It can be understood from the figure that sample S1 failed at the Al side along the border of TMAZ and HAZ. Therefore, a large proportion of Al was observed, with some fractions of Ti and Cu. Similarly, as samples S4 and S9 failed at the border of SZ and TMAZ, the elements are found according to their proportion of the mixture formed during the welding process. Finally, the sample S0 that failed along the border of TMAZ and HAZ also contained a large proportion of Al and a small fraction of Ti.

Fig. 19 SEM image of the fractured surface of specimen S1 with dimples indicating pure ductile failure
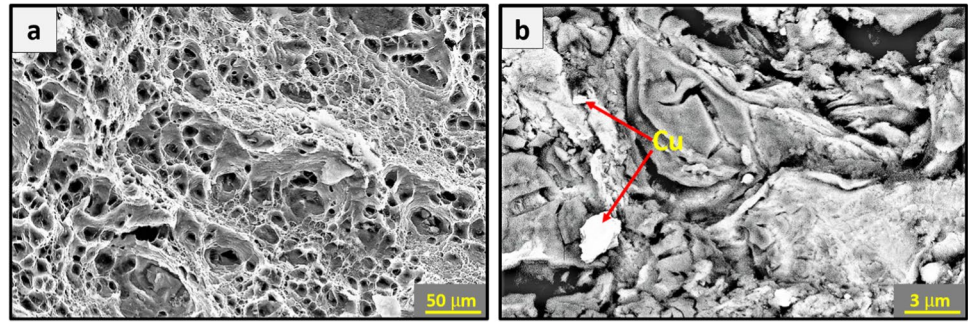

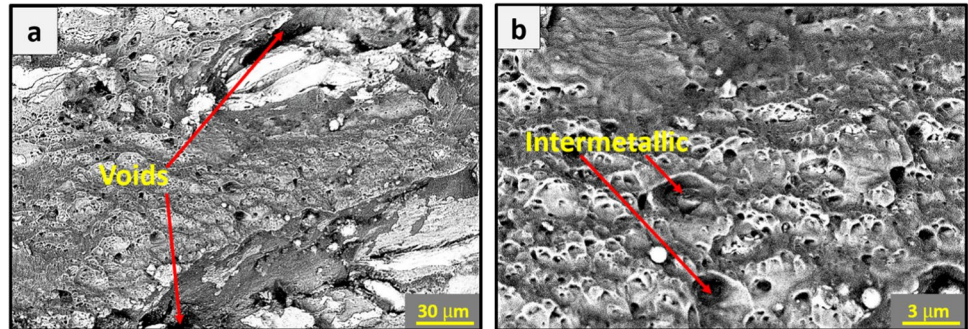**Fig. 20** SEM image of the fractured surface of specimen S4 indicating hybrid failure with few dimples

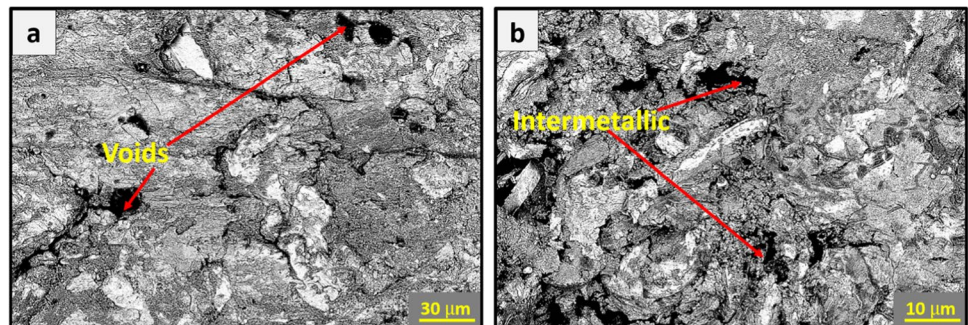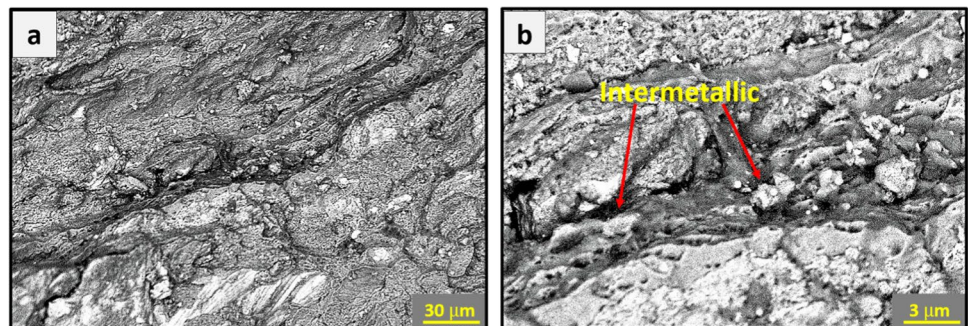**Fig. 21** SEM image of the fractured surface of specimen S9 indicating brittle intermetallics and voids

Fig. 22 SEM image of the fractured surface of specimen S0 indicating brittle intermetallics

3.7 Validation of optimal process parameters

The optimal process parameters were validated with the help of ANOVA. Figure 24 represents the main effects plots of the response variables, such as temperature on the Ti side, temperature difference, microhardness, and tensile strength.

Figure 24a shows that minimum temperature is obtained at 500 rpm tool rotation and 14 mm/min tool traverse speeds, respectively. Since both temperature rise and temperature
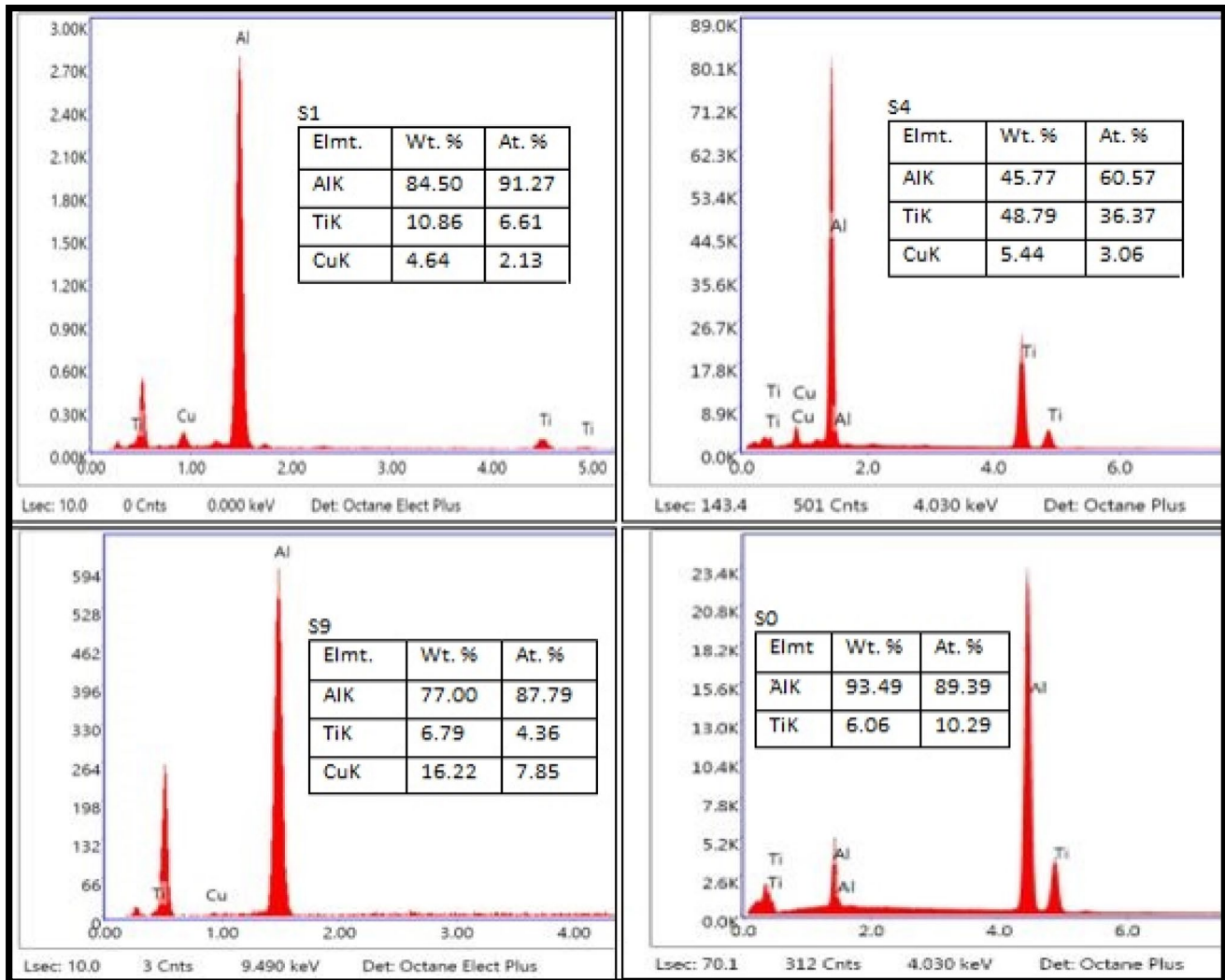
Fig. 23 The SEM–EDX of the fractured surfaces of samples S1, S4, S9, and S0

difference between Ti and Al sides are "smaller is better" type characteristics, therefore minimum value is desirable for both the response variables. A similar result is obtained from Fig. 24b as from Fig. 24a. Figure 24c and d show that the maximum hardness and tensile strength were obtained at 500 rpm and 14 mm/min of tool rotation and traverse speeds, respectively.

4 Conclusion and future scope

In this research work, sound and appropriate FSW of Al/Ti alloys with Cu interlayer was carried out successfully with the help of the tapered tool at optimal machine settings of tool rotation and traverse speeds. The use of Cu interlayer

with the metallic alloys proved significant in enhancing the joint strength by mitigating the formation of Al_3Ti intermetallics, as affirmed through the conducted experiments and obtained results duly deliberated in previous sections. The following inferences can be drawn as mentioned below:

1. The temperature rise and the temperature difference were minimum in the case of the joints welded at 500 rpm and 14 mm/min. It resulted in a balanced mixture without noticeable defects and contained negligible brittle intermetallics. On the other hand, the intermetallic Al_3Ti is formed in all the other welds due to insufficient diffusion time, higher welding temperatures, and differences.

2. The distortion and mechanical mixing of the constituents in the welded region was affected mainly by the tool
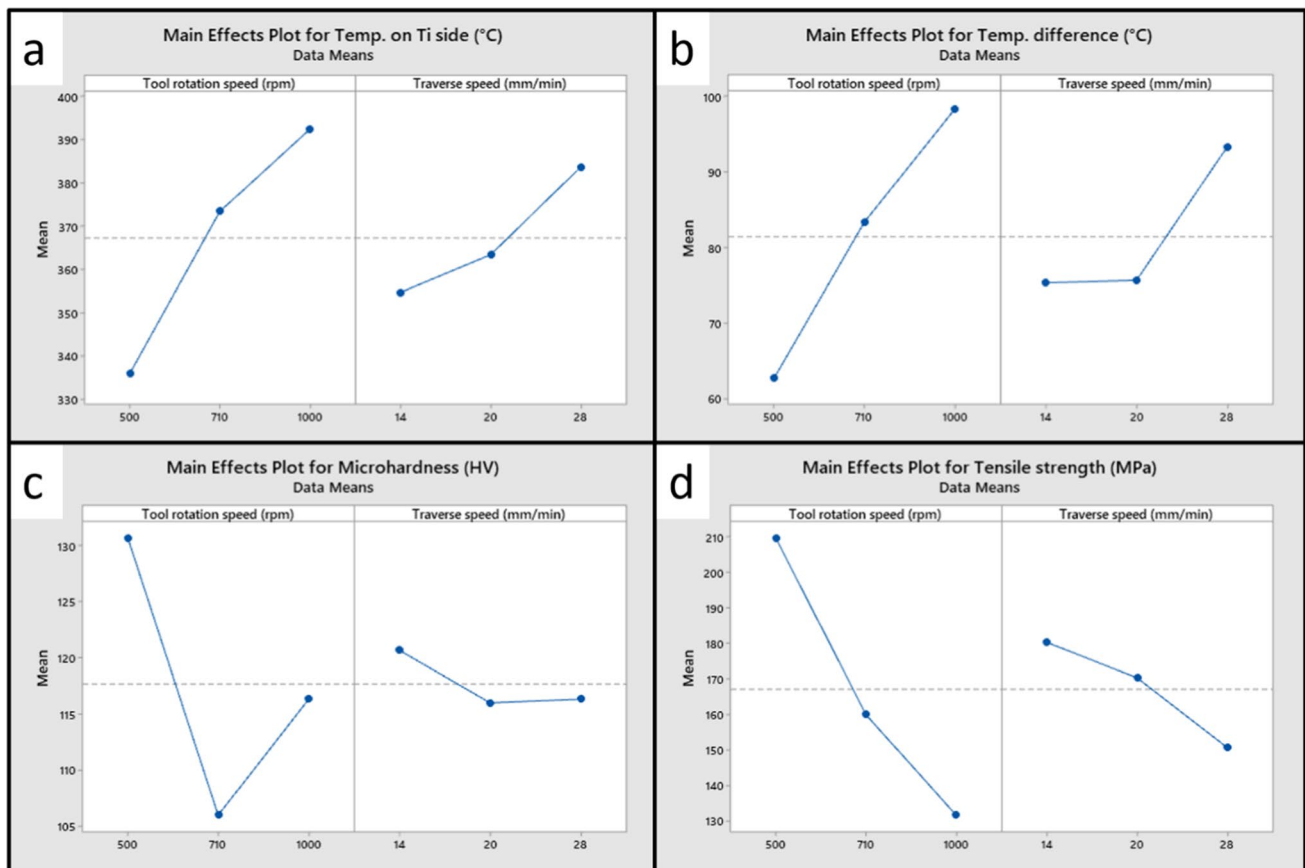
Fig. 24 Main effects plot of the responses: **a** temperature on Ti side, **b** temperature difference, **c** microhardness, and **d** tensile strength

(rpm) and (TS). Sound-quality weld was produced with lower values of the machine conditions at 500 rpm and 14 mm/min TS at a fixed tool offset. These interactions intensified with a change in offset distance, causing violent deformation and mixing and excess formation of the intermetallics.

3. In contrast, at higher values of (rpm) and (TS), worm-hole defects developed by severe mechanical mixing. The turbulent metal's drift in welding, the variation in material movement pattern, and the movement limitations of the Al alloy by other metals during joining are all attributed to the development of such flaws.

4. The ternary mixing affects the phase development in the stir zone. A negligible amount of intermetallics is observed with welding at 500 rpm and 14 mm/min TS. In this condition, Cu is mechanically mixed with Al and Ti alloys in substantial quantities, resulting in the proportion needed to make various other intermetallics that are less brittle and less harmful for producing sound-quality joints. The development of the mechanically mixed region depends on the distortion, disintegration, and dispersion of the constituents in the welded zone. The variation in welding conditions leads to diversified

scattering of intermetallics and particles in the nugget zone and varied weld properties. At higher values of welding conditions, a significant amount of the inter-metallic Al_3Ti developed in the weld. The process for developing Al_3Ti is motivated by diffusion at a higher welding temperature (> 350 °C). As less development energy is required compared to all other compounds that may potentially form at that joining temperature, Al_3Ti is the significant intermetallic present in the nugget area.

5. The maximum hardness of welded joints with interlayer at the center was about 142 HV of the joint welded at 500 rpm and 14 mm/min. There was a decreasing trend in the hardness value which is a minimum of 102 HV at 710 rpm and 20 mm/min due to large flakes of elemental Cu interlayer. The increasing trend beyond the above parameter was due to harder Al_3Ti intermetallic and large Ti particles in the weld region. The hardness at the center of the joint without interlayer was 151 HV.

6. The lowest tensile strength was found in the joints welded at 1000 rpm and 28 mm/min TS, which was correlated with the formation of larger voids and higher intermetallics. Due to inadequate mixing, the joints welded at 710 rpm, and at 1000 rpm failed in the nugget zone and had reduced

strength. The joint with the most substantial strength, near the perfect weld, and fewer intermetallics was produced at 500 rpm and failed at the boundary of TMAZ and HAZ. The highest strength of the welded joint with interlayer was recorded as much as 234 MPa, or 73% of the strength of the Al alloy joined at 500 rpm and 14 mm/min TS. The lowest was found to be 122 MPa which is only 37% of Al alloy base metal for 1000 rpm and 28 mm/min TS. The joint without an interlayer had a strength of 184 MPa.

7. The fractured weld joints with interlayer welded at 500 rpm and 14 mm/min TS were only pure ductile. Other interlayered joints at 500 rpm fractured in hybrid mode resulting in somewhat brittle and ductile fracture. Joints at 710 rpm failed as smooth surfaces due to undistorted and large elemental Cu flakes and were also brittle due to the Intermetallics of Al$_3$Ti. The rest welded at 1000 rpm were pure brittle, with large voids. The fractured joint without Cu interlayer was also in pure brittle form. The main effects plot of the response variables obtained through ANOVA validates the optimal process parameters obtained through the experiments.

Further developments in dissimilar welding with interlayers can be undertaken in the following directions as mentioned below:

1. The effect of the individual input variables on the experiment's outcome, such as temperature rise, tensile strength, and hardness, can be studied. The effect of means on response variables can be explored, and a mathematical relationship between the input and output variables can be developed through statistical tools.
2. The effect of different interlayers, such as nickel, zinc, and niobium, can be explored on the FSW of Al and Ti alloys to reduce intermetallics under different welding conditions.
3. Fatigue failure and wear behavior of Al-Ti welded joints with different interlayers can also be studied.
4. Determination of residual stresses can also be studied for the FSWed joints of the Al-Ti dissimilar alloys with interlayers.

Declarations

Competing interests The authors declare no competing interests.

References

1. Abbass MK, Hussein SK, Khudhair AA (2016) Optimization of mechanical properties of friction stir spot welded joints for dissimilar aluminum alloys (AA2024-T3 and AA 5754–H114). Arab J Sci Eng 41:4563–4572. https://doi.org/10.1007/s13369-016-2172-9
2. Gadakh VS, Badheka VJ, Mulay AS (2021) Solid-state joining of aluminum to titanium : a review. J Mater Des Appl 235(8):1757–1799. https://doi.org/10.1177/14644207211010839
3. Bang KS, Lee KJ, Bang HS, Bang HS (2011) Interfacial microstructure and mechanical properties of dissimilar friction stir welds between 6061–T6 aluminum and Ti-6%Al-4% V alloys. Mater Trans 52:974–978. https://doi.org/10.2320/matertrans.L-MZ201114
4. Aonuma M, Nakata K (2011) Dissimilar metal joining of 2024 and 7075 aluminium alloys to titanium alloys by friction stir welding. Mater Trans 52:948–952. https://doi.org/10.2320/matertrans.L-MZ201102
5. Kar A, Choudhury SK, Suwas S, Kailas SV (2018) Effect of niobium interlayer in dissimilar friction stir welding of aluminum to titanium. Mater Charact 145:402–412. https://doi.org/10.1016/j.matchar.2018.09.007
6. Balamurugan S, Jayakumar K, Subbaiah K (2021) Influence of friction stir welding parameters on dissimilar joints AA6061-T6 and AA5052-H32. Arab J Sci Eng 46:11985–11998. https://doi.org/10.1007/s13369-021-05773-7
7. Zhu Z, Lee KY, Wang X (2012) Ultrasonic welding of dissimilar metals, AA6061 and Ti6Al4V. Int J Adv Manuf Technol 59:569–574. https://doi.org/10.1007/s00170-011-3534-9
8. Miao Y, Ma Z, Yang X et al (2018) Experimental study on microstructure and mechanical properties of AA6061 / Ti-6Al-4V joints made by bypass-current MIG welding-brazing. J Mater Process Tech 260:104–111. https://doi.org/10.1016/j.jmatprotec.2018.05.019
9. Casalino G, Ostuni SD, Guglielmi P et al (2017) Optik mechanical and microstructure analysis of AA6061 and Ti6Al4V fiber laser butt weld. Opt - Int J Light Electron Opt 148:151–156. https://doi.org/10.1016/j.ijleo.2017.08.138
10. Wang P, Chen Z, Hu C et al (2020) Effects of annealing on the interface microstructures and mechanical properties of hot roll bonded Ti6Al4V / AA6061 clad sheets. Integr Med Res 9:11813–11825. https://doi.org/10.1016/j.jmrt.2020.08.070
11. Velu PS, Hynes NRJ, Vignesh NJ (2019) Joining of AA 6061/ Ti–6Al–4V with zinc interlayer using friction welding process. J Brazilian Soc Mech Sci Eng 41:1–13. https://doi.org/10.1007/s40430-019-2029-8
12. Wei Y, Aiping W, Guisheng Z, Jialie R (2008) Formation process of the bonding joint in Ti/Al diffusion bonding. Mater Sci Eng A 480:456–463. https://doi.org/10.1016/j.msea.2007.07.027
13. Wu A, Song Z, Nakata K et al (2015) Interface and properties of the friction stir welded joints of titanium alloy Ti6Al4V with aluminum alloy 6061. Mater Des 71:85–92. https://doi.org/10.1016/j.matdes.2014.12.015
14. Kimura M, Nakamura S, Kusaka M et al (2005) Mechanical properties of friction welded joint between Ti-6Al-4V alloy and Al-Mg alloy (AA5052). Sci Technol Weld Join 10:666–672. https://doi.org/10.1179/174329305X57455
15. Khanna N, Sharma P, Bharati M, Badheka VJ (2020) Friction stir welding of dissimilar aluminium alloys AA 6061–T6 and AA 8011–h14: a novel study. J Brazilian Soc Mech Sci Eng 42:1–12. https://doi.org/10.1007/s40430-019-2090-3
16. Garg A, Raturi M, Bhattacharya A (2020) Strength, failure and microstructure development for friction stir welded AA6061-T6 joints with different tool pin profiles. CIRP J Manuf Sci Technol 29:99–114. https://doi.org/10.1016/j.cirpj.2020.03.001

17. Mustafa SE, Ali M, Iqbal A et al (2021) Formulation and analysis of cost-effective environment-friendly metal cutting nanofluids using zinc oxide on turning of AISI 52100 steel using MQL. Eng Res Express 3. https://doi.org/10.1088/2631-8695/abd0e1

18. Sahu PK, Pal S (2017) Mechanical properties of dissimilar thickness aluminium alloy weld by single/double pass FSW. J Mater Process Technol 243:442–455. https://doi.org/10.1016/j.jmatprotec.2017.01.009

19. Threadgill PL (2007) Terminology in friction stir welding. Sci Technol Weld Join 12:357–360. https://doi.org/10.1179/174329307X197629

20. Hussein S, Tahir A, Al-Obaidi M (2022) Evaluation the efects of welding parameters on tri-dissimilar friction.pdf. Weld World 66:2315–2332. https://doi.org/10.1007/s40194-022-01360-y

21. Chen YC, Nakata K (2009) Microstructural characterization and mechanical properties in friction stir welding of aluminum and titanium dissimilar alloys. Mater Des 30:469–474. https://doi.org/10.1016/j.matdes.2008.06.008

22. Yu M, Zhao H, Jiang Z et al (2019) Microstructure and mechanical properties of friction stir lap AA6061-Ti6Al4V welds. J Mater Process Tech 270:274–284. https://doi.org/10.1016/j.jmatprotec.2019.03.007

23. Shehabeldeen TA, Yin Y, Ji X, Shen X (2021) Investigation of the microstructure, mechanical properties and fracture mechanisms of dissimilar friction stir welded aluminium / titanium joints. J Mater Res Technol 11:507–518. https://doi.org/10.1016/j.jmrt.2021.01.026

24. Zhou L, Yu M, Zhao H et al (2020) Dissimilar friction stir welding of AA6061 and Ti6Al4V alloys : a study on microstructure and mechanical properties. J Manuf Process 48:119–126. https://doi.org/10.1016/j.jmapro.2019.09.043

25. Yu M, Zhao H, Xu F et al (2021) Effects of ultrasonic on friction stir Al – Ti welds : a comparative study. Sci Technol Weld Join 26:551–558. https://doi.org/10.1080/13621718.2021.1968233

26. Yue Y, Zhang Z, Ji S et al (2018) Friction stir lap welding of 6061–T6 Al to Ti-6Al-4V using low rotating speed. Int J Adv Manuf Technol 96:2285–2291. https://doi.org/10.1007/s00170-018-1769-4

27. Dressler U, Biallas G, Alfaro Mercado U (2009) Friction stir welding of titanium alloy TiAl6V4 to aluminium alloy AA2024-T3. Mater Sci Eng A 526:113–117. https://doi.org/10.1016/j.msea.2009.07.006

28. Song Z, Nakata K, Wu A et al (2014) Influence of probe offset distance on interfacial microstructure and mechanical properties of friction stir butt welded joint of Ti6Al4V and A6061 dissimilar alloys. Mater Des 57:269–278. https://doi.org/10.1016/j.matdes.2013.12.040

29. Zhou L, Yu M, Zhao H et al (2019) Dissimilar friction stir welding of AA6061 and Ti6Al4V alloys: a study on microstructure and mechanical properties. J Manuf Process 48:119–126. https://doi.org/10.1016/j.jmapro.2019.09.043

30. Shankar S, Chattopadhyaya S, Mehta KP, Vilaça P (2022) Influence of copper plate positioning, zero tool offset, and bed conditions in friction stir welding of dissimilar Al-Cu alloys with different thicknesses. CIRP J Manuf Sci Technol 38:73–83. https://doi.org/10.1016/j.cirpj.2022.04.001

31. Sundar A, Kumar A, Kishore K (2022) Investigation of material flow, microstructure evolution, and texture development in dissimilar friction stir welding of Al6061 to Ti6Al4V. Mater Today Commun 33:104424. https://doi.org/10.1016/j.mtcomm.2022.104424

32. Nagu K, Kumar A (2022) Effect of brass interlayer on microstructure, mechanical and corrosion behaviour of friction stir welded AA6061-T6 alloy. Proc Inst Mech Eng Part C J Mech Eng Sci 236:5412–5427. https://doi.org/10.1177/09544062211061480

33. Abu-Okail M, Abu-Oqail A, Ata MH (2020) Effect of friction stir welding process parameters with interlayer strip on microstructural characterization and mechanical properties. J Fail Anal Prev 20:173–183. https://doi.org/10.1007/s11668-020-00813-0

34. Dong SK, Lin S, Zhu H et al (2022) Effect of Ni interlayer on microstructure and mechanical properties of Al/Mg dissimilar friction stir welding joints. Sci Technol Weld Join 27:103–113. https://doi.org/10.1080/13621718.2021.2014742

35. Peng P, Wang W, Zhang T et al (2022) Effects of interlayer metal on microstructures and mechanical properties of friction stir lap welded dissimilar joints of magnesium and aluminum alloys. J Mater Process Technol 299. https://doi.org/10.1016/j.jmatprotec.2021.117362

36. Saleh M, Liu H, Ushioda K, Fujii H (2022) Effect of Zn interlayer on friction stir butt welding of A1100 and SUS316L stainless steel. Sci Technol Weld Join 27:361–373. https://doi.org/10.1080/13621718.2022.2053398

37. Meshram SD, Madhusudhan Reddy G (2015) Friction welding of AA6061 to AISI 4340 using silver interlayer. Def Technol 11:292–298. https://doi.org/10.1016/j.dt.2015.05.007

38. Kumar R, Balasubramanian M (2015) Experimental investigation of Ti-6Al-4V titanium alloy and 304L stainless steel friction welded with copper interlayer. Def Technol. https://doi.org/10.1016/j.dt.2014.10.001

39. Mokabberi SR, Movahedi M, Kokabi AH (2018) Effect of interlayers on softening of aluminum friction stir welds. Mater Sci Eng A 727:1–10. https://doi.org/10.1016/j.msea.2018.04.093

40. Zhang Z, Huang J, Yao C, Zhang X (2022) Effect of Ag alloying on the microstructure and mechanical properties of laser welded-brazed Ti/Al dissimilar joints. Mater Sci Eng A 848:143359. https://doi.org/10.1016/j.msea.2022.143359

41. Zhang Z, Huang J, Fu J et al (2022) Microstructure and mechanical properties of laser welded-brazed titanium/aluminum joints assisted by titanium mesh interlayer. J Mater Process Technol 302:117502. https://doi.org/10.1016/j.jmatprotec.2022.117502

42. Chen YH, Ni Q, Ke LM (2012) Interface characteristic of friction stir welding lap joints of Ti/Al dissimilar alloys. Trans Nonferrous Met Soc China (English Ed) 22:299–304. https://doi.org/10.1016/S1003-6326(11)61174-6

43. Shehabeldeen TA, El-shafai NM, El-mehasseb IM et al (2021) Improvement of microstructure and mechanical properties of dissimilar friction stir welded aluminum / titanium joints via aluminum oxide nanopowder. Vacuum 188:110216. https://doi.org/10.1016/j.vacuum.2021.110216

44. Abdollah-Zadeh A, Saeid T, Sazgari B (2008) Microstructural and mechanical properties of friction stir welded aluminum/copper lap joints. J Alloys Compd 460:535–538. https://doi.org/10.1016/j.jallcom.2007.06.009

45. Xue P, Xiao BL, Ni DR, Ma ZY (2010) Enhanced mechanical properties of friction stir welded dissimilar Al-Cu joint by intermetallic compounds. Mater Sci Eng A 527:5723–5727. https://doi.org/10.1016/j.msea.2010.05.061

46. Sahu PK, Pal S, Pal SK, Jain R (2016) Influence of plate position, tool offset and tool rotational speed on mechanical properties and microstructures of dissimilar Al/Cu friction stir welding joints. J Mater Process Technol 235:55–67. https://doi.org/10.1016/j.jmatprotec.2016.04.014

47. Kar A, Suwas S, Kailas SV (2019) Significance of tool offset and copper interlayer during friction stir welding of aluminum to titanium. Int J Adv Manuf Technol 100:435–443. https://doi.org/10.1007/s00170-018-2682-6

48. Dixit S, Madhu HC, Kailas SV, Chattopadhyay K (2017) Role of insert material on process loads during FSW. Int J Adv Manuf Technol 91:3427–3435. https://doi.org/10.1007/s00170-016-9974-5

49. Li B, Zhang Z, Shen Y et al (2014) Dissimilar friction stir welding of Ti-6Al-4V alloy and aluminum alloy employing a modified butt

joint configuration: influences of process variables on the weld interfaces and tensile properties. Mater Des 53:838–848. https://doi.org/10.1016/j.matdes.2013.07.019

50. Nawaz Ahmad G, Padman J, Shahid Raza M et al (2018) Analyzing the effect of tool pin design and process parameters on the microstructural and mechanical properties of Friction Stir Welded 6061 Aluminium alloy. IOP Conf Ser Mater Sci Eng 377. https://doi.org/10.1088/1757-899X/377/1/012059

51. Biswas P, Kumar DA, Mandal NR (2012) Friction stir welding of aluminum alloy with varying tool geometry and process parameters. Proc Inst Mech Eng Part B J Eng Manuf 226:641–648. https://doi.org/10.1177/0954405411424111

52. Hynes NRJ, Velu PS (2018) Effect of rotational speed on Ti-6Al-4V-AA 6061 friction welded joints. J Manuf Process 32:288–297. https://doi.org/10.1016/j.jmapro.2018.02.014

53. Shouzheng W, Yajiang L, Juan W et al (2014) Microstructure and joining mechanism of Ti/Al dissimilar joint by pulsed gas metal arc welding. Int J Adv Manuf Technol 70:1137–1142. https://doi.org/10.1007/s00170-013-5290-5

54. Chen S, Yang D, Li M et al (2016) Laser penetration welding of an overlap titanium-on-aluminum configuration. Int J Adv Manuf Technol 87:3069–3079. https://doi.org/10.1007/s00170-016-8732-z

55. Rajakumar S, Balasubramanian V (2016) Diffusion bonding of titanium and AA 7075 aluminum alloy dissimilar joints—process modeling and optimization using desirability approach. Int J Adv Manuf Technol 86:1095–1112. https://doi.org/10.1007/s00170-015-8223-7

56. Plaine AH, Suhuddin UFH, Alcântara NG, dos Santos JF (2017) Microstructure and mechanical behavior of friction spot welded AA6181-T4/Ti6Al4V dissimilar joints. Int J Adv Manuf Technol 92:3703–3714. https://doi.org/10.1007/s00170-017-0439-2

57. Mishra RS, Ma ZY (2005) Friction stir welding and processing. Mater Sci Eng R Reports 50:1–78. https://doi.org/10.1016/j.mser.2005.07.001

58. Sujata M, Bhargava S, Sangal S (1997) On the formation of TiAl3 during reaction between solid Ti and liquid Al. J Mater Sci Lett 16:1175–1178. https://doi.org/10.1007/bf02765402

59. Song Z, Nakata K, Wu A, Liao J (2013) Interfacial microstructure and mechanical property of Ti6Al4V/A6061 dissimilar joint by direct laser brazing without filler metal and groove. Mater Sci Eng A 560:111–120. https://doi.org/10.1016/j.msea.2012.09.044

60. Barekatain H, Kazeminezhad M, Kokabi AH (2014) Microstructure and mechanical properties in dissimilar butt friction stir welding of severely plastic deformed aluminum AA 1050 and commercially pure copper sheets. J Mater Sci Technol 30:826–834. https://doi.org/10.1016/j.jmst.2013.11.007